



# Abrogating GPT2 in triple-negative breast cancer inhibits tumor growth and promotes autophagy

Devina Mitra<sup>1,2</sup> | Silvia Vega-Rubin-de-Celis<sup>1,3</sup>  | Nadine Royla<sup>4</sup> |  
 Stephan Bernhardt<sup>1,2</sup> | Heike Wilhelm<sup>1</sup> | Nooraldeen Tarade<sup>1,2</sup> |  
 Gernot Poschet<sup>5</sup> | Michael Buettner<sup>5</sup> | Ilona Binenbaum<sup>6,7,8,9</sup> |  
 Simone Borgoni<sup>1,2</sup> | Martina Vetter<sup>10</sup> | Eva Johanna Kantelhardt<sup>10</sup> |  
 Christoph Thomssen<sup>10</sup> | Aristotelis Chatziioannou<sup>7,11</sup> | Rüdiger Hell<sup>5</sup> |  
 Stefan Kempa<sup>4,12</sup> | Karin Müller-Decker<sup>13</sup> | Stefan Wiemann<sup>1,2</sup> 

<sup>1</sup>Division of Molecular Genome Analysis, German Cancer Research Center (DKFZ), Heidelberg, Germany

<sup>2</sup>Faculty of Biosciences, University of Heidelberg, Heidelberg, Germany

<sup>3</sup>Institute of Cell Biology (Cancer Research), University Hospital Essen, Essen, Germany

<sup>4</sup>Max-Delbrueck-Center for Molecular Medicine in the Helmholtz Association (MDC), Berlin Institute for Medical Systems Biology (BIMSB), Berlin, Germany

<sup>5</sup>Centre for Organismal Studies (COS), University of Heidelberg, Heidelberg, Germany

<sup>6</sup>Department of Biology, University of Patras, Patras, Greece

<sup>7</sup>Institute of Biology, Medicinal Chemistry and Biotechnology, National Hellenic Research Foundation, Athens, Greece

<sup>8</sup>Division of Medical Informatics for Translational Oncology, German Cancer Research Centre, Heidelberg, Germany

<sup>9</sup>Division of Pediatric Hematology-Oncology, First Department of Pediatrics, National and Kapodistrian University of Athens, Greece

<sup>10</sup>Department of Gynaecology, Martin-Luther-University Halle-Wittenberg, Halle (Saale), Germany

<sup>11</sup>e-NIOS PC, Athens, Greece

<sup>12</sup>Max-Delbrueck-Center for Molecular Medicine in the Helmholtz Association (MDC), Berlin Institute of Health (BIH), Berlin, Germany

<sup>13</sup>DKFZ Tumor Models Core Facility, German Cancer Research Center (DKFZ), Heidelberg, Germany

## Correspondence

Devina Mitra and Stefan Wiemann, Division of Molecular Genome Analysis, German Cancer Research Center (DKFZ), Im Neuenheimer Feld 580, 69120 Heidelberg, Germany.  
 Email: devinamitra@hotmail.com (D. M.) and s.wiemann@dkfz.de (S. W.)

## Funding information

European Union's Horizon 2020 research and innovation program, Grant/Award Number: EpiPredict - 642691; German Federal Ministry

## Abstract

Uncontrolled proliferation and altered metabolic reprogramming are hallmarks of cancer. Active glycolysis and glutaminolysis are characteristic features of these hallmarks and required for tumorigenesis. A fine balance between cancer metabolism and autophagy is a prerequisite of homeostasis within cancer cells. Here we show that glutamate pyruvate transaminase 2 (GPT2), which serves as a pivot between glycolysis and glutaminolysis, is highly upregulated in aggressive breast cancers, particularly the triple-negative breast cancer subtype. Abrogation of this enzyme results in

**Abbreviations:** Baf A1, bafilomycin A1; CRISPR/Cas9, clustered regularly interspaced short palindromic repeats/CRISPR-associated protein 9; DMSO, dimethyl sulfoxide; DKFZ, German Cancer Research Center; GC-MS, gas chromatography-mass spectrometry; GPT2, glutamate pyruvate transaminase 2; KO, knockout; METABRIC, Molecular Taxonomy of Breast Cancer International Consortium; mTORC1, mechanistic target of rapamycin complex 1; PC, pyruvate carboxylase; PDH, pyruvate dehydrogenase; PUM1, pumilio 1; qRT-PCR, quantitative real-time polymerase chain reaction; RPPA, reverse phase protein array; sgRNA, single-guide ribonucleic acid; siRNA, small interfering ribonucleic acid; TCA cycle, tricarboxylic acid cycle; TNBC, triple-negative breast cancer; Tor1, torin 1; UPLC, ultra-performance liquid chromatography;  $\alpha$ -KG,  $\alpha$ -ketoglutarate.

Devina Mitra and Silvia Vega-Rubin-de-Celis contributed equally to this study.

[Correction added on 20 January 2021, after first online publication: Projekt Deal funding statement has been added.]

This is an open access article under the terms of the Creative Commons Attribution License, which permits use, distribution and reproduction in any medium, provided the original work is properly cited.

© 2020 The Authors. *International Journal of Cancer* published by John Wiley & Sons Ltd on behalf of UICC.

of Education and Research, Grant/Award Number: e:Med - FKZ: 031A429; e:Bio - FKZ: 0316168; NCT-DKTK School of Oncology

decreased tricarboxylic acid cycle intermediates, which promotes the rewiring of glucose carbon atoms and alterations in nutrient levels. Concordantly, loss of GPT2 results in an impairment of mechanistic target of rapamycin complex 1 activity as well as the induction of autophagy. Furthermore, *in vivo* xenograft studies have shown that autophagy induction correlates with decreased tumor growth and that markers of induced autophagy correlate with low GPT2 levels in patient samples. Taken together, these findings indicate that cancer cells have a close network between metabolic and nutrient sensing pathways necessary to sustain tumorigenesis and that aminotransferase reactions play an important role in maintaining this balance.

#### KEYWORDS

autophagy, breast cancer, cancer metabolism, GPT2, mTORC1

## 1 | INTRODUCTION

Breast cancer is a heterogeneous disease and despite successes in targeted therapy of some subtypes, treatment still remains a clinical challenge.<sup>1</sup> In particular, patients with triple-negative breast cancer (TNBC) subtype, histopathologically defined as negative for protein expression of estrogen receptor, progesterone receptor and human epidermal growth factor 2, are known to have the worst prognosis and currently lack any targeted therapy. Breast cancer like several other tumor diseases undergo global metabolic shifts in order to sustain their growth and survival.<sup>2,3</sup> Elucidating metabolic changes in breast cancer, therefore, provides an opportunity to potentially overcome current therapeutic challenges. Metabolic reprogramming plays a crucial role in tumorigenesis by fulfilling the biosynthetic and bioenergetic demands for rapid growth and maintaining the redox state of tumor cells. Activated aerobic glycolysis, also known as “the Warburg effect,” is the most commonly reported metabolic characteristic in tumors.<sup>4</sup> In addition to the Warburg effect, glutamine addiction is commonly observed in several cancer types as glutamine is the second most important carbon source after glucose. This fuels the tricarboxylic acid (TCA) cycle to provide both energy and biosynthetic precursors.<sup>5</sup> Glutamine is broken down in the cells and distributed into different non-essential amino acids via transaminase reactions to produce  $\alpha$ -ketoglutarate ( $\alpha$ -KG), a key metabolite of the TCA cycle. Recent reports have shown that aminotransferase enzymes, like glutamate pyruvate transaminase 2 (GPT2), which catalyzes the reversible reaction between glucose-derived pyruvate and glutamine-derived glutamate to produce alanine and  $\alpha$ -KG, are essential for tumor growth.<sup>6,7</sup>

In addition to providing building blocks, metabolites can regulate signaling in cancer cells to promote cell growth. High cellular levels of certain amino acids including glutamine, can activate the mechanistic target of rapamycin complex 1 (mTORC1) which controls cell growth.<sup>8-11</sup> Conversely, nutrient starvation and impaired mTORC1 activity can induce self-eating in cells, a process known as macroautophagy (referred to as autophagy from here on), in order to promote cell survival.<sup>9,12,13</sup>

Our study reveals that TNBC tumors have increased GPT2 expression compared to other subtypes. While perturbations of this aminotransferase reaction decrease TCA cycle metabolites in accordance with

### What's new?

Glutamate pyruvate transaminase 2 (GPT2) serves a key role in glutaminolysis, a major feature of metabolic reprogramming in cancer, and is known to be upregulated in certain tumor types. In this study, GPT2 was found to be significantly upregulated in aggressive breast cancers, especially triple negative breast cancer (TNBC). Its downregulation, meanwhile, inhibited growth in triple-negative MDA-MB-468 cells. In addition, GPT2 inhibition reduced cellular glutamate uptake, an effect linked to GPT2 modulation of the mTORC1 pathway and autophagy activity. The findings highlight relationships between metabolic enzymes, nutrient signaling and autophagy in breast cancer, potentially opening up new therapeutic opportunities.

its role in anaplerosis, we also observed a decrease in glutamine uptake and rewiring of glucose carbon atoms in cells concomitant with abrogated alanine synthesis. Furthermore, we found that the observed metabolic changes result in an inactivation of mTORC1 as well as in the induction of autophagy both *in vitro* and *in vivo*. This connection between GPT2 and nutrient sensing pathways (autophagy and mTORC1) was also present in patients suggesting that there is a strong network between these pathways which collectively supports tumorigenesis. Loss of GPT2 inhibits tumor growth also *in vivo*, corroborating GPT2 as a critical enzyme in oncogenesis in TNBC by playing a crucial role in maintaining a balance between opposing nutrient sensing mechanisms.

## 2 | MATERIALS AND METHODS

### 2.1 | Patient samples

Tissue lysates from fresh-frozen breast cancer patient samples were derived from the multicenter prospective Prognostic assessment in

routine Application (PIA, NCT01592825) as previously described.<sup>14</sup> Breast cancer subtypes were defined to histopathological characteristics such as receptor status and grading according to the St Gallen classification and by von Minckwitz and colleagues.<sup>15,16</sup> Expression of proteins was analyzed by reverse phase protein array (RPPA).

## 2.2 | Cell culture

MDA-MB-468 (RRID:CVCL\_0419) and MCF7 (RRID:CVCL\_0031) cell lines were purchased from ATCC (LGC Standards GmbH, Wesel, Germany) and grown in RPMI 1640 media supplemented with 10% FCS. Cells were cultured at 37°C in a humidified atmosphere and 5% CO<sub>2</sub>.

Both parental cell lines as well as the GPT2 knock outs have been repeatedly authenticated using single nucleotide polymorphism (SNP) profiling (Multiplexion GmbH, Friedrichshafen, Germany). All experiments were performed with mycoplasma-free cells.

## 2.3 | Small interfering ribonucleic acid and inhibitor treatment

Prior to small interfering ribonucleic acid (siRNA) transfections, cells were seeded to 80% confluency. After overnight cultivation, transfections were performed with RNAiMax (Invitrogen AG, Carlsbad, Kalifornien) according to the manufacturer's instructions. siRNAs (Dharmacon, Lafayette, Colorado) were used at a final concentration of 10 nM (sequences: Table S1).

For inhibitor treatment, cells were seeded to 60% confluency. After overnight cultivation, cells were treated with inhibitors: GPT2 inhibitor ( $\beta$ -chloro-L-alanine hydrochloride, Sigma-Aldrich, Saint-Louis, Missouri, CAS 2731-73-9), bafilomycin A1 (Baf A1, VWR, Radnor, Pennsylvania), torin 1 (Tor1, TargetMol, Boston, Massachusetts) diluted in growth media. Water or dimethyl sulfoxide (DMSO; for Baf A1 and Tor1) were used as controls. Cells were incubated in 37°C, 5% CO<sub>2</sub> humidified atmosphere for different time points depending on the assay being performed.

## 2.4 | Gene targeting

GPT2 knockout (KO) clones were generated with CRISPR/Cas9 technology. Single-guide RNAs (sgRNAs) targeting exon 4 of GPT2 gene (sequences: Table S2) and Cas 9 were obtained from Synthego (Synthego Corporation, Menlo Park, California). Cells were seeded to 80% confluency and were transfected with Lipofectamine CRISPRMAX Cas 9 transfection reagent (Thermo Fisher Scientific, Waltham, Massachusetts) the following day according to the manufacturer's instructions.

## 2.5 | Quantitative real-time polymerase chain reaction analysis

RNA was isolated using the RNeasy Mini Kit (Qiagen, Hilden, Germany) according to the manufacturer's recommendations. For

quantification, 1  $\mu$ g of total RNA was reverse transcribed using the RevertAid H minus First strand Kit and the resulting cDNA was used as template in polymerase chain reaction (PCR). Taqman based assays were used for quantitative real-time PCR (qRT-PCR). Primers and universal probe library (UPL) probes (Roche Diagnostics GmbH, Mannheim, Germany) were designed using the Roche UPL Design Center (Roche Diagnostics GmbH) (sequences: Table S3). Raw data were analyzed using SDS software and the  $\Delta\Delta$ Ct method.<sup>17</sup> Ct values were normalized to the housekeeping gene pumilio 1 (PUM1).

## 2.6 | Microarray

Genome-wide gene expression profiling was performed using HumanHT-12 v4 BeadChips (Illumina, San Diego, California). Raw probe intensities were background-corrected using negative control probes and a normal + exponential (normexp) convolution model. An offset value (=16) was added to the data in order to prevent negative gene expression in the background correction step. Data were then normalized via quantile normalization using the negative and positive probes.<sup>18</sup> Control probes were removed and intensities log<sub>2</sub>-transformed after normalization. The German Cancer Research Center (DKFZ) microarray core facility performed sample preparation, RNA quality control and hybridization.

The *lumi* R package<sup>19</sup> was used for processing, quality control, background correction and robust spline normalization of gene expression data. The *limma* R package<sup>20</sup> was used for testing of differential gene expression. Functional analysis and gene prioritization were performed using BioInfoMiner<sup>21</sup> (<https://bioinforminer.com>) as well as by pathway enrichment analysis and visualization using the gene set enrichment analysis (GSEA)<sup>22</sup> module on the GenePattern platform.<sup>23</sup>

## 2.7 | Protein expression analysis

Cells were lysed on ice with ice-cold M-PER lysis buffer (Pierce, Bonn, Germany) containing protease (Complete Mini, Roche, Mannheim, Germany) and phosphatase inhibitors (PhosSTOP, Roche, Mannheim, Germany). Cell lysates were incubated on a tube rotator for 30 minutes at 4°C and subsequently centrifuged for 10 minutes at 16000g. Total protein concentration was quantified with a Pierce BCA Protein Assay Kit according to the manufacturer's instructions (Thermo Fisher Scientific). Protein expression was analyzed by immunoblotting and RPPA.

## 2.8 | Immunoblotting

Protein isolates were denatured using 4 $\times$  Roti Load (Roth-Chemie GmbH, Karlsruhe, Germany) for 5 minutes at 95°C and 20  $\mu$ g of total protein was separated on in 12.5% SDS PAGE. Proteins were blotted onto PVDF Immobilon-P membranes (Merck, Darmstadt, Germany). Membranes were blocked for 60 minutes at room temperature (RT) in Rockland blocking buffer, then primary antibodies (see Table S4) were incubated overnight at 4°C in Rockland blocking buffer. After three

washing steps with TBS-T, secondary IRDye680 or IRDye800 conjugated antibodies (LI-COR, Lincoln, Nebraska) were diluted 1:10000 in Tris-buffered saline supplemented with Tween-20 (TBS-T) was purchased from Pierce (Thermo Scientific, Waltham, MA) and incubated with the membranes for 45 minutes at RT. Membranes were scanned and analyzed with an Odyssey scanner and Odyssey 2.1 software, respectively (LI-COR). For Western blot quantification, local background subtraction and  $\beta$ -actin normalization was performed.

## 2.9 | RPPA profiling

The method used in this study has been described previously.<sup>24</sup> Briefly, cell lysates were adjusted to a total protein concentration of 2  $\mu\text{g}/\mu\text{L}$ , mixed with 4 $\times$  SDS sample buffer (10% glycerol, 4% SDS, 10 mM DTT, 125 mM Tris-HCl, pH 6.8) and denatured at 95°C for 5 minutes. Lysates were spotted on nitrocellulose-coated glass slides (Grace-Biolabs, Bend, Oregon) using an Aushon 2470 contact spotter (Aushon BioSystems, Billerica, Massachusetts). Spotted slides were incubated with blocking buffer (Rockland Immunochemicals, Gilbertsville, Pennsylvania) in TBS (50%, v/v) containing 5 mM NaF and 1 mM  $\text{Na}_3\text{VO}_4$  for 2 hours at room temperature, prior to incubation with target-specific primary antibodies at 4°C overnight. Primary antibodies were detected with either Alexa Fluor 680-coupled goat anti-mouse or anti-rabbit IgG, each in a 1:8000 dilution (Life Technologies, Darmstadt, Germany). In addition, every ninth slide was stained with the Fast Green FCF protein dye for total protein quantification, as described before.<sup>24</sup> TIFF images of all slides were obtained at an excitation wavelength of 685 nm and at a resolution of 21  $\mu\text{m}$  using an Odyssey Scanner (LI-COR). Signal intensities of individual spots were quantified using GenePixPro 7.0 (Molecular Services Inc., Sunnyvale, California). Data preprocessing, merging of technical triplicates, background correction and quality control were performed using the RPPAnalyzer R-package.<sup>25</sup>

## 2.10 | Cell proliferation assay

Cell growth under different treatment conditions was analyzed by microscopic counting of nuclei. Cells were seeded in 96-well plates with flat bottom black polystyrene wells (Greiner Bio-One International GmbH, Kremsmuenster, Austria). After overnight incubation, cells were transfected with siRNAs or treated with inhibitors. DNA was stained with intercalating dye Hoechst-33 258 (Sigma-Aldrich) at the indicated time points at a 1:1000 dilution in growth media, for 45 minutes. Subsequently, plates were imaged with a high content screening microscope (IXM XLS, Molecular Devices, Sunnyvale, California). All nuclei were defined by Hoechst signals within a certain size and intensity range and were detected and counted using Molecular Devices Software.

## 2.11 | Alanine assay

GPT2 inhibitor (BCLA) titration was done by measuring the alanine levels in the supernatants using an alanine assay kit (Sigma). Five

microliters of 1:10 diluted supernatants were used in the assay following the manufacturer's instructions.

## 2.12 | Measurement of extracellular alanine, glutamine, glucose and lactate

To analyze the content of amino acids, 10  $\mu\text{L}$  of cell culture supernatant was mixed with 290  $\mu\text{L}$  of ice-cold 0.1 M HCl. Insoluble material and proteins were precipitated by centrifugation for 10 minutes at 25000g. Five microliters of the supernatant were used for labeling with the fluorescence dye AccQ-TagTM (Waters, Milford, Massachusetts) according to the manufacturer's protocol. Labeled metabolites were separated by reversed-phase chromatography using an Acquity BEH C18 column (150 mm  $\times$  2.1 mm, 1.7  $\mu\text{m}$  diameter, Waters) connected to an Acquity H-class ultra-performance liquid chromatography (UPLC) system and quantified by fluorescence detection (Acquity FLR detector, Waters, excitation: 250 nm, emission: 395 nm) using ultrapure standards (Sigma-Aldrich). The column was heated to 42°C and equilibrated with 5 column volumes of buffer A (140 mM sodium acetate pH 6.3, 7 mM triethanolamine) at a flow rate of 0.45 mL/min. Baseline separation of amino acid derivatives was achieved by increasing the concentration of acetonitrile (B) in buffer A as follows: 1 minute 8% B, 7 minutes 9% B, 7.3 minutes 15% B, 12.2 minutes 18% B, 16.3 minutes 40% B, 18.5 minutes 80% B, hold for 3 minutes and return to 8% B in 3 minutes. Data acquisition and processing were performed with the Empower3 software suite (Waters).

For determination of organic acids, cations and sugars, supernatants were diluted with ultra-pure water before analysis. For sugar determination, samples were diluted 1:1000. For organic acids as well as for cations a 1:30 dilution was used. Organic acids were separated using an IonPac AS11-HC (2 mm, Thermo Fisher Scientific) column connected to an ICS-5000 system (Thermo Fisher Scientific) and quantified by conductivity detection after cation suppression (ASRS-300 2 mm, suppressor current 95-120 mA). Prior to separation, the column was heated to 30°C and equilibrated with 5 column volumes of solvent A (ultra-pure water) at a flow rate of 0.38 mL/min. Separation of anions and organic acids was achieved by increasing the concentration of solvent B (100 mM NaOH) in buffer A as follows: 8 minutes 4% B, 18 minutes 18% B, 25 minutes 19% B, 43 minutes 30% B, 53 minutes 62% B, 53.1 minutes 80% B for 6 minutes and return to 4% B in 11 minutes. Data acquisition and quantification were performed with chromeleon 7 (Thermo Fisher Scientific). Extracellular organic acid measurements from KO cells were done with gas chromatography-mass spectrometry (GC-MS) analysis.

## 2.13 | Isotope labeling and metabolite measurement for inhibitor experiments

### 2.13.1 | Labeling and harvest

Cells were plated with a predetermined cell number to reach a similar confluency after 48 hours of incubation. Twenty-four hours after

plating, the GPT2 inhibitor was added and incubation continued for another 24 hours. Four hours prior to harvesting, 1 mL of medium was collected to determine all secreted metabolites. The remaining media was discarded and cell culture continued with fresh media containing <sup>13</sup>C-glucose (Campro Scientific, Berlin, Germany). After an incubation for 30 minutes, adherent cells were quickly flushed with wash buffer (140 mM NaCl, 5 mM HEPES, pH 7.4 supplemented with glucose and glutamine) to remove extracellular metabolites but not the main carbon sources. Then, cells were instantly quenched with 5 mL ice-cold 50% methanol (supplemented with cinnamic acid [final concentration: 2 µg/mL]). Cells were scratched, collected, and transferred into a 15-mL Falcon tube and stored as well as the media samples at -20°C until proceeding with metabolite extraction.

### 2.13.2 | Intracellular extraction

One milliliter chloroform was added to 5 mL of methanolic cell extracts, shaken for 60 minutes at 4°C and centrifuged at 4149g for 15 minutes at 4°C for phase separation (methanol-chloroform-water extraction). Polar phases were collected and dried under vacuum. Cell extracts were stored at -20°C until preparation for GC-MS analysis.

### 2.13.3 | Extracellular extraction

One milliliter of methanol-chloroform-water (5:2:1, v/v/v, supplemented with cinnamic acid [final concentration: 2 µg/mL]) was added to 50 µL of media samples, shaken for 30 minutes at 4°C. Five hundred microliters of H<sub>2</sub>O were added, and samples were centrifuged at 4149g for 15 minutes at 4°C for phase separation. Two times 500 µL of polar phase were collected and dried under vacuum. The extracellular extracts were stored at -20°C until preparation for GC-MS analysis. Extracellular amino acids were measured accordingly using UPLC.

### 2.13.4 | GC-MS analysis

A quantification dilution series was treated in parallel with the extracts. Derivatization was carried out as previously described with modifications.<sup>26</sup> Dried cell extracts were dissolved in 20 µL of methoxyamine hydrochloride solution (Sigma-Aldrich, 40 mg/mL in pyridine [Roth Chemie GmbH, Karlsruhe, Germany]) and incubated for 60 minutes at 30°C with constant shaking followed by the addition of 80 µL of *N*-methyl-*N*-[trimethylsilyl]trifluoroacetamide (Machery-Nagel, Dueren, Germany) and incubation for 90 minutes at 37°C. The extracts were centrifuged for 10 minutes at 10 000g and aliquots of 30 µL each were then transferred into glass vials (Th. Geyer, Berlin, Germany) for GC-MS measurement.

Metabolite analysis was performed via gas chromatography coupled to a time-of-flight mass spectrometer (Pegasus III-TOF-MS-System, LECO Corp., St. Joseph, Michigan), equipped with an auto-

sampler (MultiPurpose Sampler 2 XL, Gerstel, Mülheim an der Ruhr, Germany). Samples were injected in split mode (split 1:5, injection volume 1 µL) in a temperature-controlled injector (CAS4, Gerstel) with a baffled glass liner (Gerstel). The following temperature program was applied during sample injection: initial temperature of 80°C for 30 seconds followed by a ramp with 12°C/min to 120°C and a second ramp with 7°C/min to 300°C and final hold for 2 minutes. Gas chromatographic separation was performed on an Agilent 6890N (Agilent, Santa Clara, California), equipped with a VF-5 ms column of 30 m length, 250 µm inner diameter and 0.25 µm film thickness (Varian, Palo Alto, California). Helium was used as carrier gas with a flow rate of 1.2 mL/min. Gas chromatography was performed with the following temperature gradient: 2 minutes heating at 70°C, first temperature gradient with 5°C/min up to 120°C and hold for 30 seconds; subsequently, a second temperature increase of 7°C/min up to 350°C with a hold time of 2 minutes. The spectra were recorded in a mass range of 60 to 600 U with 20 spectra/s at a detector voltage of 1650 V.

GC-MS chromatograms were processed using ChromaTOF software (LECO Corp.). Mass spectra data were extracted using the software tool MetMax (<http://gmd.mpimp-golm.mpg.de/apps/metmax/>) or the in-house software Maui-VIA.<sup>27</sup> Mass isotope distributions of unlabeled metabolites were used to determine the <sup>13</sup>C-glucose-derived stable isotope incorporation of <sup>13</sup>C in metabolites of interest. Absolute quantities were determined by examination of the peak area in the GC-MS-derived chromatograms and their comparison to quantification standards. Acquired data were normalized to the internal standard cinnamic acid, the sum of area per sample and cell count. Aliquots of flash-frozen cell culture supernatants were used for absolute quantification of amino acid, cation, organic acid and sugar content each.

### 2.14 | GFP-LC3 assay

Cells were transfected with a GFP-LC3 plasmid (provided by Prof. Noboru Mizushima<sup>28</sup>) using Lipofectamine 2000 (Invitrogen AG) according to manufacturer's recommendations. Twenty-four hours later, cells were seeded into clear bottom black 96-well plates, incubated with respective reagents indicated in the text and then fixed in 4% PFA. Autophagosome numbers (GFP-LC3 puncta per cell) were counted with a high content screening microscope, IXM XLS (Molecular Devices). Then, 100 cells/well in triplicate were counted in each experiment.

### 2.15 | HiBiT-LC3 assay

Cells were transfected with LC3 HiBiT reporter vector (Promega, Madison, Wisconsin) using Lipofectamine 2000 (Invitrogen AG) according to the manufacturer's recommendations. Forty-eight hours posttransfection, cells were split and further culture was done with Geneticin (Life Technologies) selection. For detection of HiBiT activity, cells were seeded in white 96-well plates with media lacking Geneticin. Following treatments, as mentioned in respective figure

legends, cells were incubated with a mixture of Nano-Glo HiBIT lytic buffer, LgBIT Protein and Nano-Glo HiBIT lytic substrate (all from Promega) according to the manufacturer's recommendations and luminescence was measured using a microplate reader (Infinite M200 microplate reader, Tecan Group, Mannedorf, Switzerland).

## 2.16 | Xenograft assay

All animal experiments were performed in accordance with approved guidelines of the local Governmental Committee for Animal Experimentation (RP Karlsruhe, Baden-Württemberg, Germany). Mice were maintained at a 12-hour light-dark cycles with unrestricted Kliba 3307 diet and tap water. Under isoflurane inhalation anesthesia (1%-1.5% in O<sub>2</sub>, 0.5 L/min),  $2.5 \times 10^6$  MDA-MB-468 cells suspended in 30  $\mu$ L of PBS/growth factor-reduced Matrigel (1:1, v/v) (BD, Heidelberg, Germany) were injected into the mammary gland fat pads of 6- to 7-week-old female NOD SCID gamma (NSG) mice (n = 12) obtained from the Center for Preclinical Research (DKFZ, Heidelberg, Germany). Tumor volumes were measured with a caliper and calculated according to the formula:  $V = (\text{length [mm]} \times \text{width [mm]}^2)/2$ .

## 2.17 | Statistical analysis and graphical illustrations

Unless otherwise mentioned, data are presented as mean  $\pm$  SD. Statistical analyses were performed applying the unpaired two-tailed Student's *t* test and *P* values <.05 were considered statistically significant. *P* values <.05, <.01 and <.001 are indicated with one, two and three asterisks, respectively, in respective figures. All graphs were generated using the GraphPad Prism Software and illustrated via Inkscape v 1.0.1.

Additional materials and methods information can be found in Appendix S1.

## 3 | RESULTS

### 3.1 | GPT2 is upregulated in TNBC

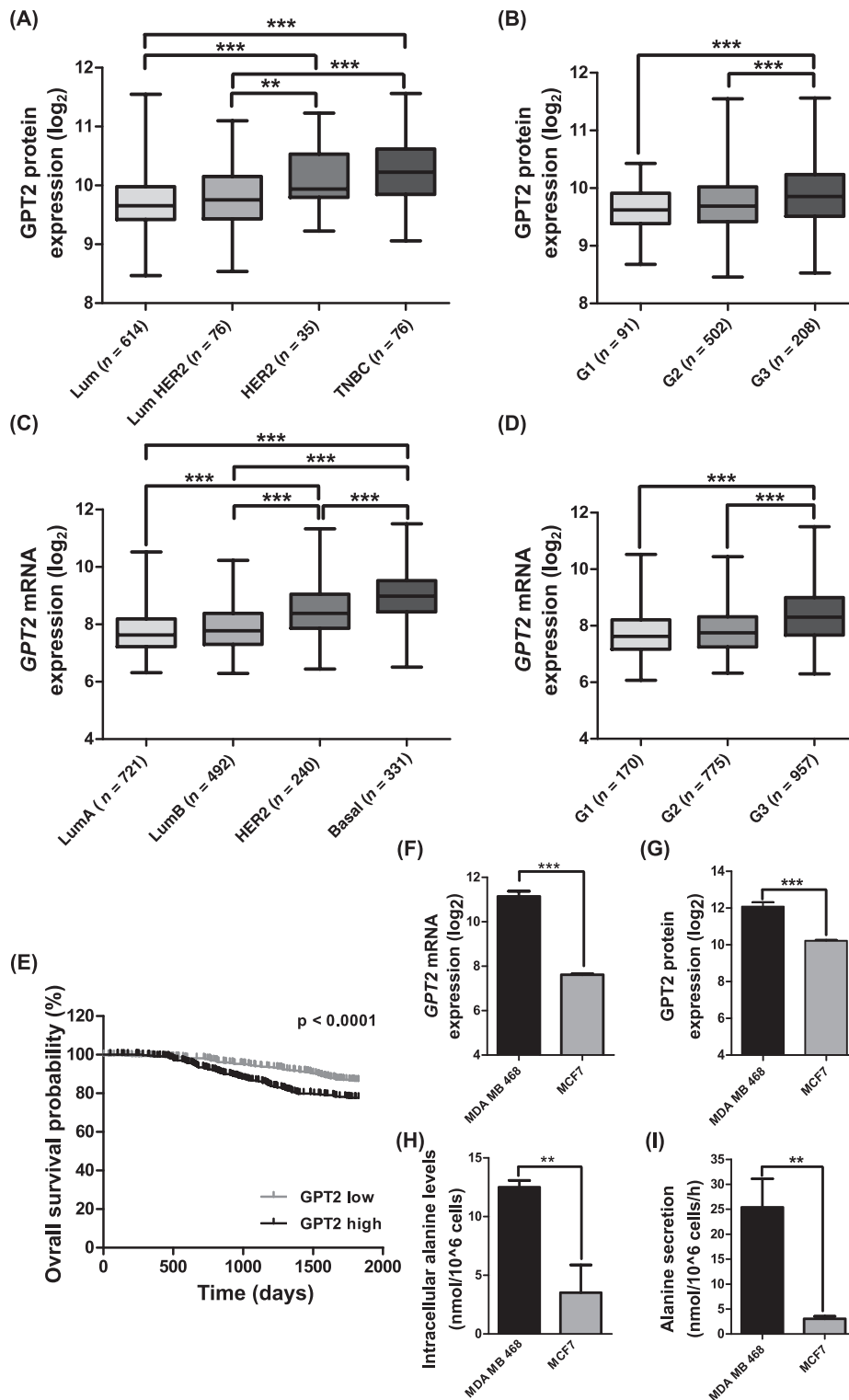
Upregulated glutamine metabolism is one of the characteristics of the TNBC subtype of breast cancer.<sup>29,30</sup> Along these lines, we found the enzyme GPT2 to be significantly higher expressed in TNBC tumors as compared to the other breast cancer subtypes (Figure 1A) within a proteomic data set of a prospective multicenter cohort of 800 breast cancer patients, the PiA cohort.<sup>14</sup> GPT2 protein expression correlated also with tumor grade (Figure 1B). These results corroborated observations made in the analysis of mRNA expression data from the Molecular Taxonomy of Breast Cancer International Consortium (METABRIC)<sup>31</sup> (Figure 1C,D) and The Cancer Genome Atlas<sup>32</sup> (Figure S1A) cohorts, where the basal subtype (most of which are classified as TNBCs) showed the highest GPT2 expression. These findings support the hypothesis that increased glutamine metabolism is a feature particularly of aggressive tumors. Indeed, Kaplan-Meier analysis

of the METABRIC data set revealed that higher GPT2 expression negatively correlates with overall patient survival (Figure 1E). A similar correlation of GPT2 expression, but not of GPT1 expression with subtypes was observed also in an expression data set of 41 breast cancer cell lines<sup>33</sup> and GPT1 expression was low compared to that of GPT2 in the MDA-MB-468 cell line (Figure S1B,C). Based on these data, we selected MDA-MB-468 and MCF7 cell lines for further analysis, since these cell lines express GPT2 at rather high and low levels and are models for the triple-negative/basal-like and luminal subtypes, respectively. GPT2 mRNA expression was lower in MCF7 compared to MDA-MB-468 (Figure 1F) thus validating the expression data from the cell line panel.<sup>33</sup> In addition, MCF7 cells also had lower GPT2 protein expression in comparison to MDA-MB-468, corroborating the mRNA data (Figure 1G). Accordingly, both intracellular and extracellular alanine levels were lower in MCF7 compared to the MDA-MB-468 cell line (Figure 1H,I). Tracing the conversion of uniformly labeled <sup>13</sup>C glucose revealed that label incorporation into the alanine pool was significantly higher in MDA-MB-468, further validating the above obtained data (Figure S1D). Taken together these data suggest that upregulated alanine metabolism correlates with increased tumor aggressiveness and is particularly elevated in the triple-negative subtype of breast cancer, both in vitro and in vivo.

### 3.2 | GPT2 downregulation inhibits cell growth in triple-negative MDA-MB-468 cells

Next, we explored whether GPT2 has an impact on tumor cell growth. To this end we followed three complementary approaches. First, we transiently knocked down GPT2 using a pool of siRNAs and observed a reduction in the relative numbers of MDA-MB-468 (Figure 2A,B) but not of MCF7 cells (Figure S3A,B). siRNA deconvolution was performed to rule out off-target effects in the MDA-MB-468 cells (Figure S2C) and similar effects were observed with the individual siRNAs. Knockdown efficiency was confirmed both at the mRNA and protein levels (Figure S2A,B). Next, cells were treated with a chemical inhibitor of alanine aminotransferase,  $\beta$ -chloro-L-alanine. The lowest effective dose was first determined for each cell line by inhibitor titration (Figures 2C and S3C) and 75 and 100  $\mu$ M were selected for MDA-MB-468 and MCF7, respectively, for subsequent experiments. Protein analysis confirmed that the inhibitor did not affect GPT2 protein levels (Figures 2E and S3E). Yet, cell growth was more strongly affected in MDA-MB-468 compared to MCF7 cells despite using a lower concentration of the inhibitor (Figures 2F and S3F,G). These data suggest that MDA-MB-468 cells are more dependent on the GPT2-catalyzed pathway than MCF7 cells. Finally, we knocked out GPT2 in MDA-MB-468 cells using CRISPR/Cas9 and two different sgRNAs each targeting exon 4 of the GPT2 gene, thus generating two independent KO cell lines, GPT2 KO1 and GPT2 KO2. Loss of GPT2 protein was confirmed by western blot analysis as well as by quantification of alanine levels in the cell supernatants (Figure 2G,H). In concordance with the other perturbations, growth of MDA-MB-468 cells with GPT2 KO was decreased (Figure 2I).

**FIGURE 1** GPT2 is upregulated in basal breast cancer and correlates with poor survival. Box plots showing GPT2 protein expression according to, A, molecular subtypes and, B, tumor grades in the PiA data set ( $n = 801$ ).<sup>14</sup> Box plots showing GPT2 mRNA expression in the METABRIC data set<sup>31</sup> according to, C, molecular subtypes ( $n = 1784$ ) and, D, tumor grades ( $n = 1902$ ). E, Kaplan-Meier survival analysis (OS) of patients in the METABRIC cohort. GPT2 expression in MDA-MB-468 and MCF7 cell lines as assessed using microarray for mRNA, F, and RPPA for protein levels, G. H, GC-MS measurements for intracellular alanine levels and, I, UPLC analysis of alanine secretion for MDA-MB-468 ( $n = 4$ ) and MCF7 ( $n = 3$ ) cell lines. Data are represented as mean  $\pm$  SD. \*\* $P < .01$ , \*\*\* $P < .001$ ,  $t$  test. GC-MS, gas chromatography-mass spectrometry; METABRIC, Molecular Taxonomy of Breast Cancer International Consortium; UPLC, ultra-performance liquid chromatography



### 3.3 | GPT2 perturbation decreases glutamine uptake and TCA cycle intermediates in TNBC cells

GPT2 is a component of the central carbon metabolism. Having observed phenotypic effects of GPT2 inhibition, we thus wanted to ascertain whether inhibition of GPT2 would directly impact this core network in vitro. Chemical inhibition of GPT2 in MDA-MB-468 cells indeed significantly reduced glutamine uptake (Figure 3A), in

agreement with previous data from colorectal cancer.<sup>7</sup> This effect was also seen upon knocking down or knocking out the gene (Figure 3B, C). As glucose contributes to the carbon skeleton of alanine we next examined whether the uptake of glucose was affected by GPT2 inhibition. While inhibitor treatment slightly increased glucose uptake, the effects of knockdown or KO of GPT2 were mostly not significant, except for GPT2 KO1 cells (Figure 3A-C). Additionally, there was a trend for decrease in the secretion of lactate, which is a readout for

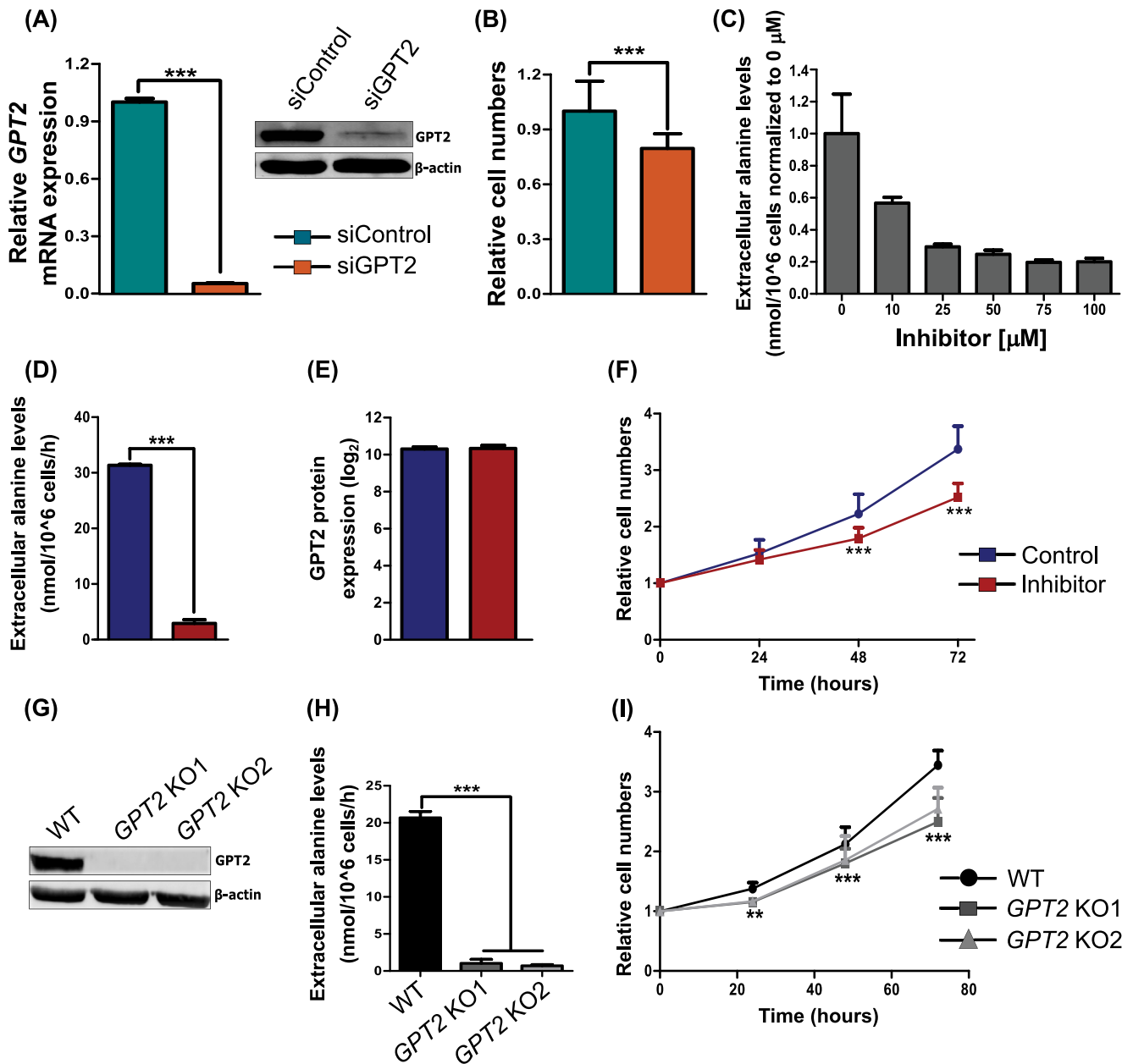


**FIGURE 2** Abrogation of GPT2 inhibits cell growth in MDA-MB-468. MDA-MB-468 cells were transfected with a pool of four siRNAs targeting *GPT2* (or corresponding nontargeting control) and then *GPT2* was quantitated by qRT-PCR and western-blot at RNA and protein levels, respectively, A, and for changes in relative cell numbers, B. *GPT2* inhibitor effects on extracellular alanine levels, C,D, *GPT2* protein expression, E, and relative cell number, F, were analyzed. G, *GPT2* was knocked out using two different sgRNAs (KO1, KO2) and *GPT2* protein levels and impact on extracellular alanine levels, H, as well on cell proliferation, I, assessed. Data are represented as mean  $\pm$  SD,  $n = 3$  biological replicates unless stated otherwise. \*\* $P < 0.01$ , \*\*\* $P < .001$ ,  $t$  test. KO, knockout; qRT-PCR, quantitative real-time polymerase chain reaction; sgRNA, single-guide ribonucleic acid

glycolysis in the cells (Figure 3A-C). Again, this decrease was significant only in *GPT2* KO1 which is in line with the decreased glucose uptake observed in these cells (Figure 3C).

In contrast, the TCA cycle intermediates, including  $\alpha$ -KG, fumarate and malate were strongly decreased upon *GPT2* inhibition, while pyruvate and citrate did not change significantly (Figure 3D). Decreases in TCA cycle intermediates were also seen in cell lines where *GPT2* had been knocked out (Figure S4C). Given that the  $\alpha$ -KG

that is generated in the reaction catalyzed by *GPT2* directly feeds into the TCA cycle thus bypassing pyruvate and citrate, these data confirm that the observed effect on the TCA cycle is a result of blockage of the *GPT2*-catalyzed transaminase reaction. In contrast to MDA-MB-468, no significant changes in the uptake of the carbon sources, glucose and glutamine, and lactate secretion were observed in MCF7 cells having been treated with the *GPT2* inhibitor (Figure S4A). The TCA cycle intermediates also did not exhibit similar dramatic changes



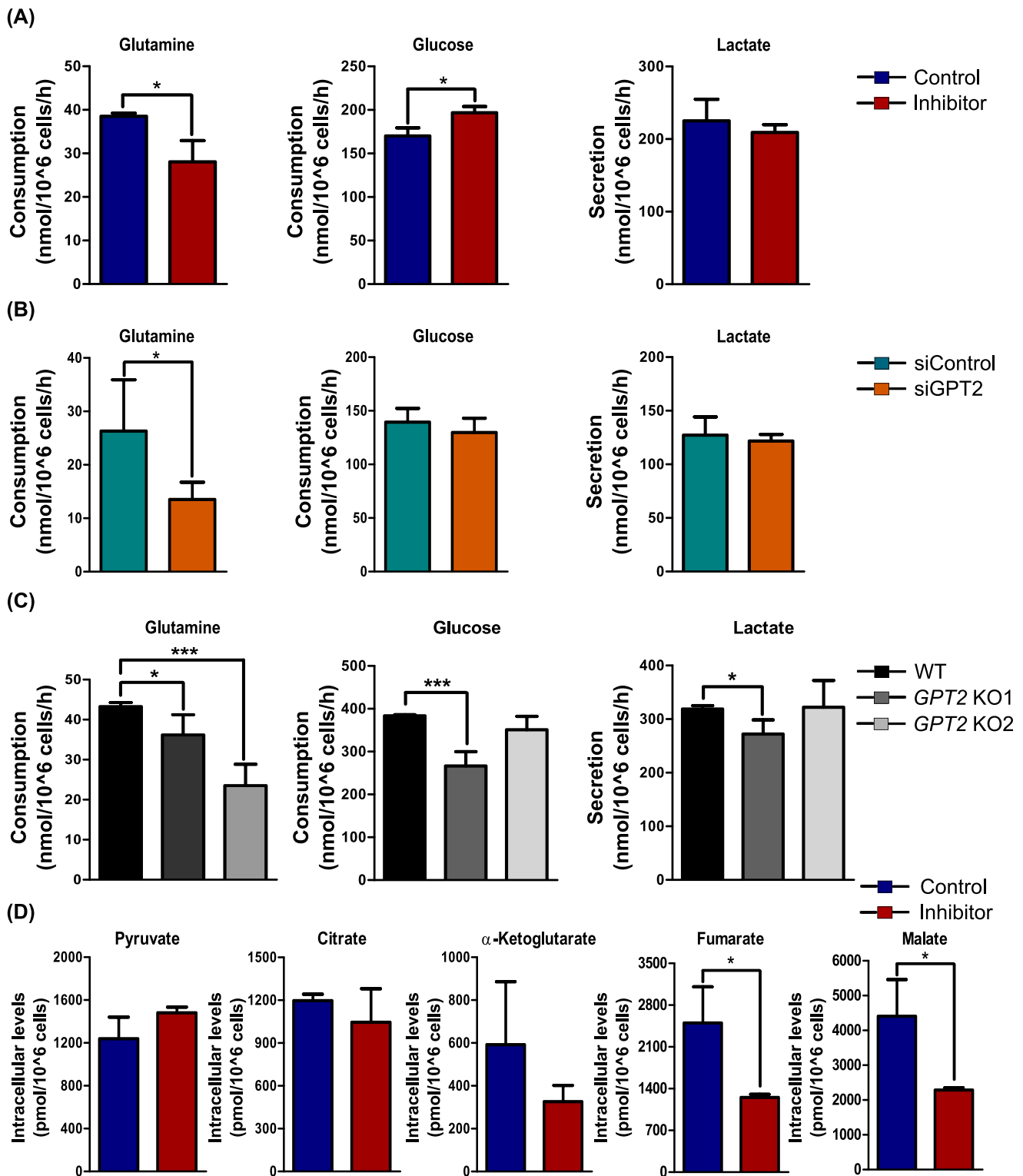


**FIGURE 3** Chemical or genetic inhibition of GPT2 decreases glutamine uptake and TCA cycle intermediates. A, UPLC analysis of glutamine and glucose consumption, and of lactate secretion in MDA-MB-468 cells, 24 hours posttreatment with GPT2 inhibitor (75  $\mu$ M) (or corresponding water control), B, 48 hours posttransfection with siGPT2 or corresponding nontargeting control ( $n = 4$ ), and, C, 48 hours postseeding of two different GPT2 knockout clones ( $n = 4$ ). D, GC-MS analysis of indicated intracellular metabolites 24 hours posttreatment of MDA-MB-468 cells with GPT2 inhibitor  $\beta$ -chloro-L-alanine (75  $\mu$ M). Data are represented as mean  $\pm$  SD,  $n = 3$  biological replicates unless stated otherwise. \* $P < .05$ , \*\*\* $P < .001$ ,  $t$  test. GC-MS, gas chromatography-mass spectrometry; TCA, tricarboxylic acid; UPLC, ultra-performance liquid chromatography

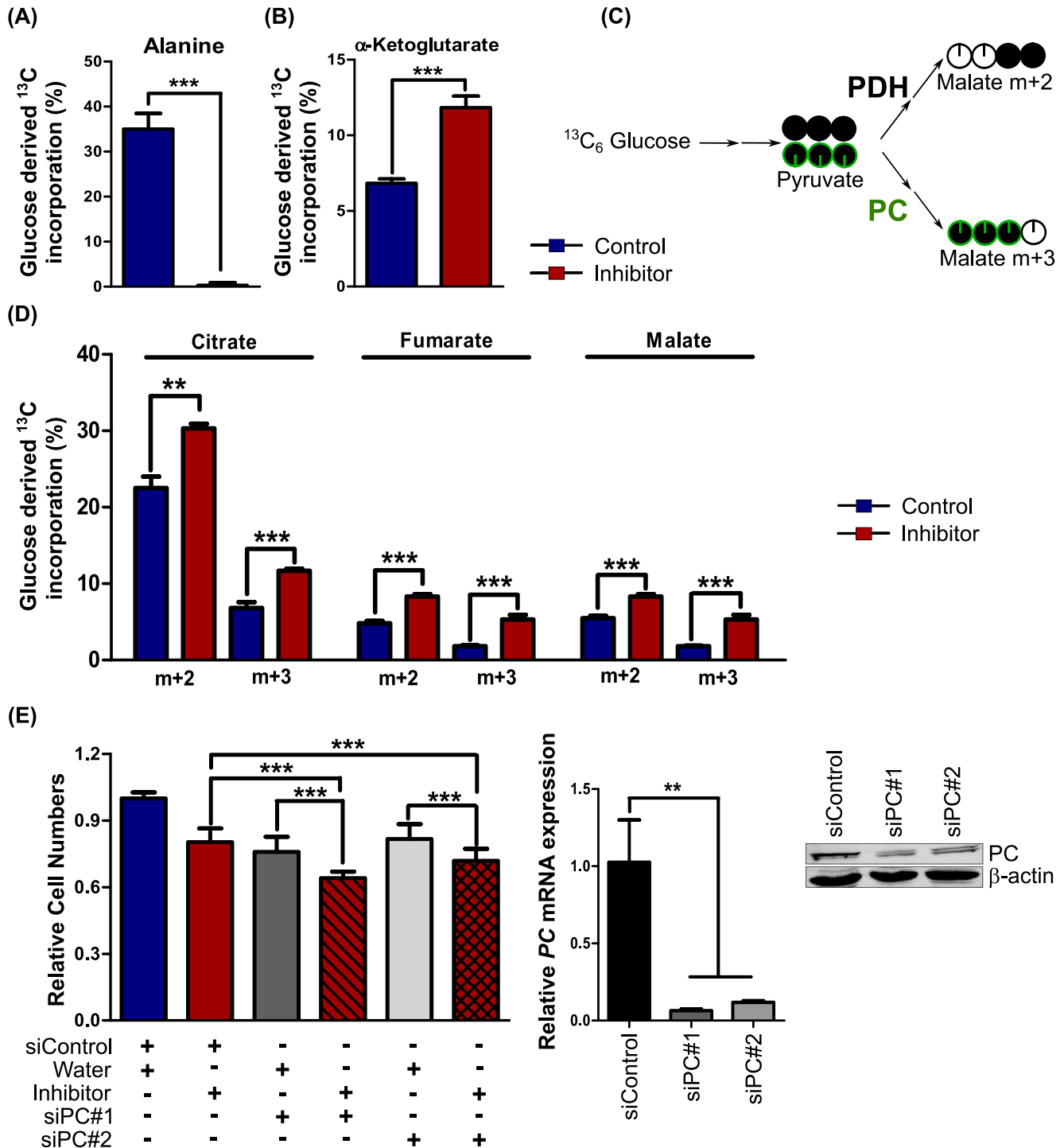


**FIGURE 4** GPT2 inhibition rewire glucose metabolism. Percentage of labeled alanine, A, and  $\alpha$ -ketoglutarate, B, pools in MDA-MB-468 cells 24 hours post treatment with GPT2 inhibitor  $\beta$ -chloro-L-alanine (75  $\mu\text{M}$ ) (or corresponding water control) and 30 minutes incubation with media supplemented with  $^{13}\text{C}$ -glucose, as measured by GC-MS. C, Schematic showing the contribution of PDH and PC catalyzed pathways to carbon atoms in malate. D, Percentage of labeled pools of metabolite detected upon treatment of MDA-MB-468 cells treated with DMSO (Control) or  $\beta$ -chloro-L-alanine (75  $\mu\text{M}$ ). E, Relative MDA-MB-468 cell numbers 72 hours after transfection with siRNA targeting PC (or corresponding nontargeting control) and treatment with GPT2 inhibitor  $\beta$ -chloro-L-alanine (75  $\mu\text{M}$ ) (or water control) (left), qRT-PCR (center) and western blot analysis (right) of PC mRNA (data represented as mean  $\pm$  SD of three biological and three technical replicates each) and protein expression, respectively, 72 hours posttransfection. Data are represented as mean  $\pm$  SD,  $n = 3$  biological replicates unless stated otherwise,  $***P < .01$ ,  $***P < .001$ ,  $t$  test. DMSO, dimethyl sulfoxide; PC, pyruvate carboxylase; PDH, pyruvate dehydrogenase; qRT-PCR, quantitative real-time polymerase chain reaction

in MCF7 as were seen in MDA-MB-468 cells, only fumarate and malate showed a small yet significant increase (Figure S4B). Thus, blocking this transaminase pathway reduces glutamine uptake as well

as TCA cycle intermediate levels in the triple-negative cell line MDA-MB-468 but does not significantly affect TCA cycle metabolism in the luminal cell line MCF7, further supporting the concept that the former

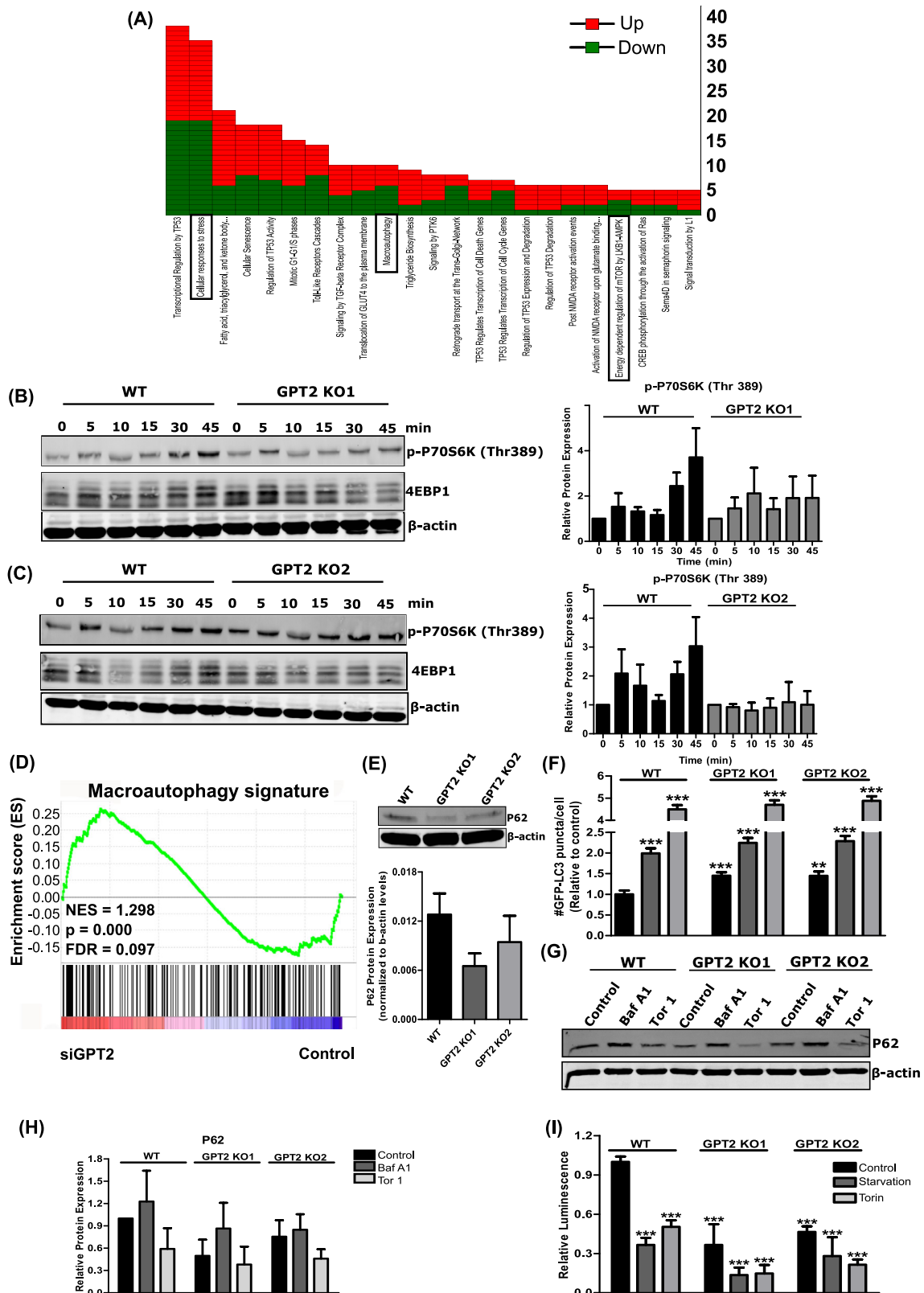


**FIGURE 5** Legend on next page.

is highly dependent on the GPT2-catalyzed pathway to sustain cell growth.

### 3.4 | GPT2 inhibition rewires glucose metabolism

Given that glucose uptake was only slightly increased upon GPT2 inhibition while lactate secretion was not elevated (Figure 3A-C), we hypothesized that the carbon atoms from glucose might lead to a buildup of cellular pyruvate levels. This might then enter into the TCA cycle and thereby compensate for the decreased input of glutamine-derived carbon atoms. As we indeed observed a trend toward increased pyruvate production upon inhibitor treatment (Figure 3D), we next traced the conversion of  $u$ - $^{13}\text{C}$ -glucose within the TCA cycle intermediates.  $^{13}\text{C}$  incorporation into alanine was indeed fully abrogated upon inhibitor treatment confirming efficient inhibition of GPT2 in MDA-MB-468 cells (Figure 4A). In contrast, labeling of  $\alpha$ -KG was strongly increased upon GPT2 inhibition, suggesting an increased contribution of glucose to replenish the metabolite pool in the TCA cycle (Figure 4B).

Pyruvate may enter the TCA cycle by reactions that are catalyzed by either pyruvate dehydrogenase (PDH) or pyruvate carboxylase (PC) producing citrate and oxaloacetate, respectively. Feeding of MDA-MB-468 cells with uniformly labeled glucose allowed us to discriminate between the respective input reactions (Figure 4C). Indeed, while all measured TCA cycle intermediates showed increased carbon incorporation from glucose upon GPT2 inhibition (Figure 4B,D), increases were most prominent in the labeled  $m + 3$  fractions of malate and fumarate (Figure 4D) pointing at a prominent PC activity. Citrate  $m + 3$  fractions, which originate both from PC and PDH (when cells undergo multiple rounds of TCA cycle) catalyzed reactions, also increased significantly. Further determination of the  $^{13}\text{C}$ -labeled quantities showed that the  $^{13}\text{C}$ -labeled pool sizes of malate and fumarate  $m + 3$  fractions as well as of citrate  $m + 3$  fractions were increased upon inhibition of GPT2. In contrast, the pool sizes for  $m + 2$  fractions exclusively originating from the PDH reaction remained unchanged (Figure S5A).

Upon GPT2 inhibition, MCF7 cells showed small but significant increases in the  $^{13}\text{C}$  incorporation of fumarate and malate, while  $^{13}\text{C}$

incorporation into citrate and  $\alpha$ -KG remained unchanged or was decreased, respectively (Figure S5B).  $^{13}\text{C}$ -labeled pool sizes of malate and fumarate  $m + 2$  fractions were higher in inhibitor-treated cells, confirming that blockage of the GPT2 pathway increasingly shunts glucose carbon atoms into the TCA cycle pathway (Figure S5C), likely via PDH and PC.

The results obtained with MDA-MB-468 cells suggest that upon GPT2 inhibition, the PC-catalyzed input into the TCA cycle might be required to compensate for the lack of carbon flow within the TCA cycle that is caused by decreased glutamine uptake. This let us test next whether combinatorial targeting of GPT2 and PC would have an enhanced effect on cell growth. Even though the knockdown of PC was efficient at the RNA level, this was not reflected at the protein level (Figure 4E) pointing to a long half-life of the enzyme or to selection for cells having higher levels of PC protein. Yet, cell numbers were significantly decreased upon knockdown of PC in combination with inhibition of GPT2, as compared to individual perturbations of either PC or GPT2 (Figure 4E). Combined treatment of GPT2 inhibition and PC knockdown had significant effects also in MCF7; however, these (Figure S5D) were smaller than in MDA-MB-468 cells, which is in agreement with the milder effects inhibition of GPT2 had in MCF7.

### 3.5 | GPT2 downregulation compromises mTORC1 activity and induces autophagy in TNBC cells

We next aimed to determine pathways connected to GPT2 and alterations in glutamine consumption. To this end, we transiently knocked down GPT2 in MDA-MB-468 cells and then profiled global gene expression. Pathway analysis indicated stress response, autophagy and mammalian target of rapamycin (mTORC1) pathways among the most differentially regulated upon knockdown of GPT2 (Figure 5A). Previous studies have shown that amino acid starvation, especially of glutamine, triggers stress pathways and autophagy of cells.<sup>8,12,34</sup> Thus, we sought to unravel whether mTORC1 activity was compromised also in our cell systems. For this purpose, mTORC1 activity was blocked by amino acid deprivation followed by amino acid repletion at different time points. MDA-MB-468 GPT2-WT cells demonstrated

**FIGURE 5** GPT2 downregulation impairs mTORC1 activity and increases autophagy in triple-negative breast cancer cells MDA-MB-468. A, Pathway analysis of differentially expressed genes from MDA-MB-468 cells transfected with siRNA targeting GPT2 or corresponding nontargeting control. B,C, Western blot analysis of phospho-p70S6K (Thr389) and total 4EBP1 protein levels (left panels), and quantification of phospho-p70S6K (Thr389) (right panels) of MDA-MB-468 WT cells and two GPT2 KO clones having been deprived of amino acid for 50 minutes followed by replenishment of amino acids for the indicated times. D, GSEA analysis of microarray data of MDA-MB-468 cells transfected with siRNA targeting GPT2 (or corresponding nontargeting control) showing core enriched distribution of macroautophagy genes, FDR = 9.8%. E, Western blot analysis of p62 protein levels (top) and quantification (bottom) in MDA-MB-468 WT and two independent clones with GPT2 KO. F, Quantification of GFP-LC3 puncta (autophagosome numbers) in WT and two independent GPT2 CRISPR/Cas9 KO clones (normalized to WT control-treated cells) ( $n = 2$  biological replicates). Western blot analysis of P62 protein levels and, G, relative protein expression of p62 protein in MDA MB 468 WT and two independent GPT2 CRISPR/Cas9 KO clones, H, treated with Baf A1 (100 nM), torin 1 (Tor1; 250 nM) or DMSO control for 3 hours. Western blot images are representative of three independent experiments. I, Relative luminescence levels (normalized to WT control treated cells) in two independent GPT2 CRISPR/Cas9 KO clones stably transfected with a HiBiT-LC3 reporter and treated with DMSO control, starvation media (HBSS) or Torin 1 (250 nM) for 3 hours. Data are represented as mean  $\pm$  SD,  $n = 3$  biological replicates unless stated otherwise. \*\*\* $P < 0.001$ , \*\* $P < 0.01$ , t-test. Baf A1, bafilomycin A1; KO, knockout; mTORC1, mechanistic target of rapamycin complex 1. FDR, false discovery rate; GSEA, gene set enrichment analysis; HBSS, Hank's Balanced Salt Solution

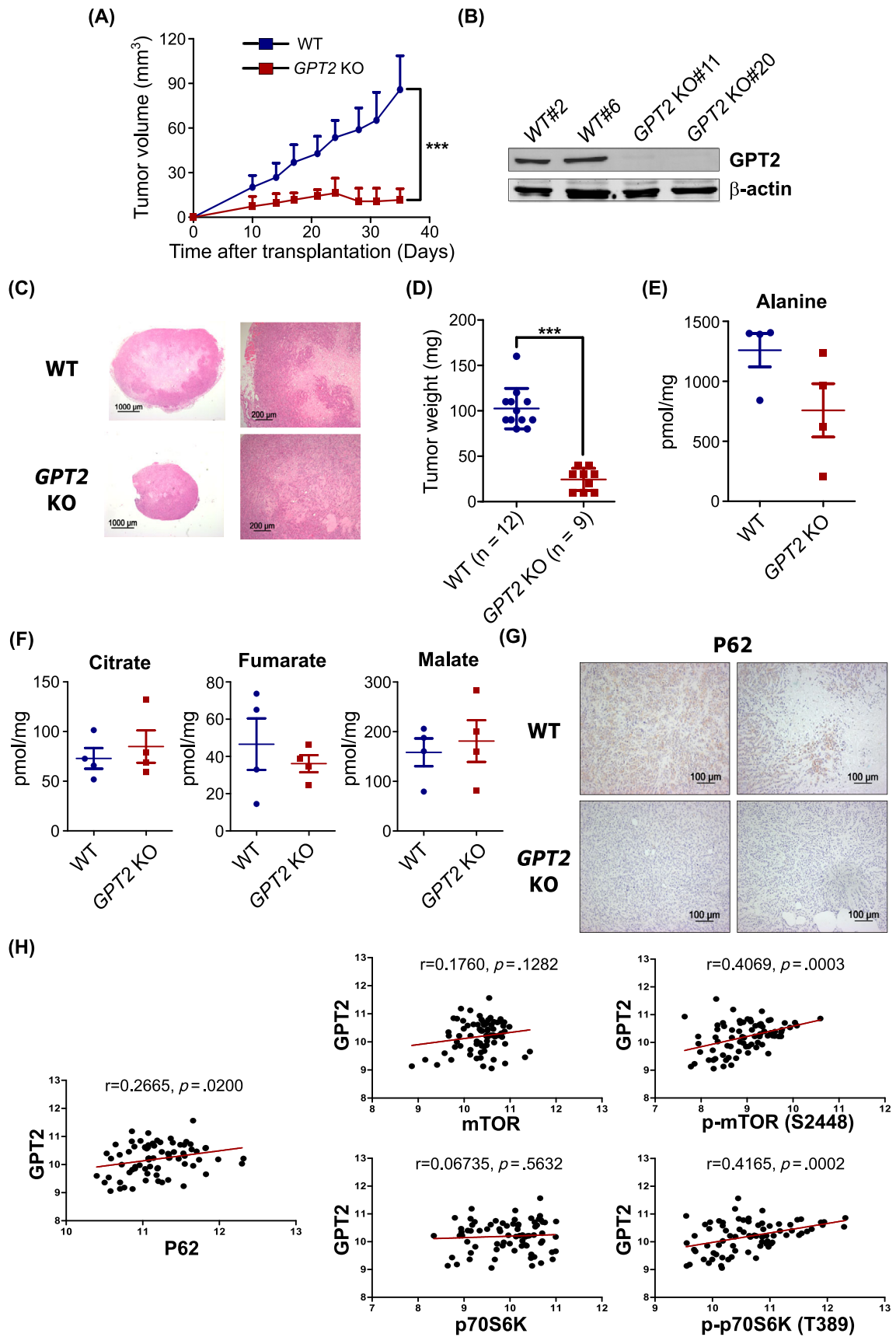


**FIGURE 6** Legend on next page.

faster recovery after amino acid repletion compared to KO cells, as shown by the increase in phosphorylation of the mTORC1 substrate p70s6K (Figure 5B,C) as well as an enrichment of hyperphosphorylated 4EBP1 protein (Figures 5B,C and S6D). These data suggested that KO of *GPT2* compromises mTORC1 activity.

Gene set enrichment analysis of the gene expression data sets revealed that knockdown of *GPT2* also exhibited an enhanced autophagy profile in vitro (Figure 5D). mTORC1 is one of the major autophagy regulators and its inhibition by amino acid starvation has been described to induce autophagy.<sup>9</sup> Thus, we next explored the status of the autophagy pathway upon *GPT2* modulation. To this end, we assessed the levels of the autophagy marker p62 by western blot, as well as of autophagosome formation using the GFP-LC3 reporter in *GPT2*-WT and KO cells. Indeed, p62 protein levels were decreased in both *GPT2* KO cell lines (Figure 5E) while the basal number of GFP-LC3 puncta was elevated (Figure 5F), suggesting an increase in autophagy activity in the absence of *GPT2* and therefore corroborating our findings from global gene expression analysis. All cells responded similarly to autophagy modulation by starvation with HBSS or inhibition of mTOR by Tor1. The relative levels of p62 were consistently lower in the KO cells; however, this was also because the basal levels of p62 were decreased in *GPT2* KO cells (Figure 5G,H). We confirmed these data using the luminescence HiBIT-tagged LC3 reporter<sup>35</sup> in stably transfected MDA-MB-468 cells (both WT and *GPT2* KO cell lines). Our results indicated that LC3 protein levels were lower all *GPT2* KO cells compared to WT control cells in all conditions tested (Figure 5I), further proving that autophagy is upregulated in cells lacking *GPT2*. Taken together these results suggest that a decrease in intracellular amino acid levels that is caused by blockage of alanine production and subsequent uptake of glutamine, indeed leads to reduced mTORC1 activity and to the activation of autophagy, potentially helping the cells to overcome the shortage of amino acids.

### 3.6 | *GPT2* KO suppresses tumor growth and induces autophagy in vivo

To assess the physiological significance of our in vitro results, we next explored the effects a loss of *GPT2* has in vivo. To this end, MDA-MB-468 WT and *GPT2* KO cells were orthotopically injected into NSG mice. Indeed, *GPT2* KO xenografts exhibited significantly and drastically slower tumor growth (Figures 6A and S6A) as well as reduced tumor weight (Figures 6D and S6B) compared to the WT

cells, with *GPT2* KO1 having a stronger effect than *GPT2* KO2 cells. KO of *GPT2* in the tumors was confirmed by western blot and this was accompanied by decreased alanine levels (Figure 6B,E). In agreement with the in vitro data (Figure 3D), citrate levels remained unchanged while fumarate levels showed a trend toward decreasing in *GPT2* KO xenografts compared to the WT, while malate levels were not affected (Figures 6F and S6C). Also consistent with our in vitro results, p62 levels were lower in the *GPT2* KO xenografts, suggesting an induction of autophagy in *GPT2* KO tumors as well (Figure 6G).

Finally, we tested a potential correlation between *GPT2* expression and autophagy in patients and quantified the levels of autophagy-related proteins in tumors of the PiA cohort.<sup>14</sup> Indeed, the expression level of p62 was positively correlated with *GPT2* in TNBC tumors (Figure 6H), but not in the other subtypes (Figure S6E). As expected, the phosphorylated forms of mTOR and p70s6k proteins strongly correlated with *GPT2* expression in TNBC tumors, whereas the total proteins did not (Figure 6H). Interestingly, the positive correlation of *GPT2* expression we observed with phosphorylated mTOR as well as p70s6k proteins was even stronger in the other subtypes of breast cancer, suggesting that the link between mTOR signaling and *GPT2* could be relevant in breast cancer in general. These findings thus substantiate the connection between mTORC1 activity and glutaminolysis in breast cancer, while that between *GPT2* and autophagy might be specific for the TNBC subtype (Figure S6E). To our knowledge, this is the first report (a) providing quantitative analysis of *GPT2* in breast cancer patients at the protein level; (b) presenting in vivo data from CRISPR *GPT2* KO cells; and (c) uncovering the correlation between *GPT2* and autophagy as well as mTORC1 activity in vitro, in vivo and in patients.

## 4 | DISCUSSION

Metabolic reprogramming is an essential part of tumorigenesis, which is prominently characterized by the Warburg effect and glutamine anaplerosis.<sup>2,3,36</sup> Glutamine-dependent growth is an important feature of several aggressive cancers including the TNBC subtype.<sup>2,3,36,37</sup> In our study, we found that *GPT2*, which is part of a network of enzymes involved in glutaminolysis, is significantly upregulated in aggressive breast cancers, especially in the triple-negative subtype. Its expression negatively correlates with overall patient survival. Of note, this is the first study showing *GPT2* expression not only at the mRNA but also at

**FIGURE 6** *GPT2* KO suppresses tumor growth. A, Xenograft tumor growth of MDA-MB-468 WT cells and two independent *GPT2* KO clones (n = 12 each group). B, Western blot analysis of *GPT2* protein expression in two representative WT and *GPT2* KO tumors. C, Representative images of H&E-stained tumor tissue sections. D, Scatter plot of tumor weights in the WT MDA-MB-468 and *GPT2* KO xenograft groups. E, UPLC measurements of alanine levels in WT and *GPT2* KO xenografts. F, GC-MS analysis of metabolite levels in WT and *GPT2* KO tumors. G Representative images of p62 in IHC analysis of tissue sections from WT and *GPT2* KO tumors. H, Correlation between *GPT2* protein and indicated autophagy-related proteins in TNBC patients (n = 76) in the PiA patient cohort.<sup>14</sup> Data are represented as mean ± SD, n = 4 biological replicates unless stated otherwise. \*\*\*P < .001 t test. Correlation coefficients (r) and significance were calculated using Pearson's correlation test. GC-MS, gas chromatography-mass spectrometry; PiA, Prognostic assessment in routine Application; UPLC, ultra-performance liquid chromatography; TNBC, triple-negative breast cancer

the protein levels. These clinical findings corroborate our in vitro data showing that perturbation of *GPT2* expression in triple-negative MDA-MB-468 cells slows down cell growth. Blocking the alanine aminotransferase reaction results in a reduced glutamine uptake. This is in line with previous studies having shown that the alanine aminotransferase reaction positively correlates with glutamine uptake.<sup>6,7,38</sup> Cancer cells utilize aminotransferase reactions to feed glutamine-derived carbons into the TCA cycle via  $\alpha$ -KG along a major route of glutamine catabolism. Here, we have observed that inhibition of *GPT2* results in reduced  $\alpha$ -KG pools and that this reduction is concurrent with a decrease in the pool of TCA cycle intermediates downstream of  $\alpha$ -KG, thus confirming this transamination reaction to be an important anaplerotic route.<sup>6,7,38</sup> We cannot completely rule out targeting also of other enzymatic reactions by the chemical inhibitor we applied.<sup>39</sup> However, the strong overlap of metabolic and phenotypic effects we observed upon inhibition and knockdown/KO of *GPT2* suggests that, indeed, the main activity of  $\beta$ -chloro-L-alanine seems to be on the inhibition of the alanine aminotransferase reaction that is catalyzed by *GPT2* in our system. This conclusion is supported by the finding that *GPT1*, a paralog of *GPT2* and a second target of  $\beta$ -chloro-L-alanine, is neither expressed in the MDA-MB-468 cell line nor in other breast cancer cell lines at similar levels as *GPT2*.

*GPT2* is a pivotal enzyme linking glutamine catabolism and glycolysis.<sup>6</sup> However, the fate of carbon atoms in glucose has not been explored thus far in conditions of abrogated *GPT2* activity. Our data illustrate that inhibition of *GPT2* results in an increased carbon flow from glucose into the TCA cycle possibly to compensate for the reduction in TCA cycle metabolites. We also show that despite having a weaker impact on luminal cell line MCF7, *GPT2* inhibition induces similar effects on glucose rewiring also in these cells. Interestingly, we found that the TCA cycle intermediates deriving from pyruvate carboxylation were significantly increased upon *GPT2* inhibitor treatment in MDA-MB-468 cells suggesting that PC activity is elevated upon *GPT2* inhibition. Furthermore, combinatorial targeting of *GPT2* and PC had an even stronger effect on cell growth compared to the individual treatments. PC has been shown to play a key role in anaplerosis under glutamine starvation conditions,<sup>40</sup> and another study showed that lung metastases from breast cancer switch from the glutamine to PC anaplerotic routes in response to changes in the tumor microenvironment.<sup>41</sup> These studies support our finding that tumor cells tend to upregulate pyruvate carboxylation upon reduced glutamine uptake, potentially to support biosynthetic processes. However, our data suggest that this mechanism is not sufficient to maintain cellular homeostasis.

Nutrient starvation is counteracted by different cellular mechanisms, one major process being autophagy (self-eating) where the cells undergo partial proteolysis enabling them to replenish their pool of amino acids.<sup>12,42,43</sup> However, only few amino acids can trigger autophagy, including glutamine.<sup>8-11</sup> Our data illustrate this connection as we found an enrichment of autophagy pathway genes and an induction of autophagosome formation in *GPT2* KO cells. Amino acid deprivation also leads to inactivation of mTORC1 thereby triggering autophagy.<sup>9-11,13</sup> Consistent with this, we found that KO of *GPT2*

results in decreased mTORC1 activity as seen by the reduced phosphorylation levels of downstream effectors of the pathway, p70s6k and 4EBP1.<sup>44,45</sup>

Our in vitro findings were substantiated upon in vivo testing, as growth of xenograft tumors was massively impeded in the absence of *GPT2*. The even stronger growth impairment seen in vivo might be due to several factors including longer duration of the experiment where cells undergo many more rounds of replication. Furthermore, glutamine could become a limiting factor in vivo as physiological levels are lower than in cell culture.<sup>10,46</sup> More research is needed to investigate these and potential other factors affecting tumor growth in conditions where *GPT2* activity is abrogated. The observed reduction in p62 levels in the KO tumors indicates that autophagy activation likely occurs as an adaptation to the loss of *GPT2* also in vivo. These results are further supported by patient data where we could show a strong correlation between *GPT2* protein levels and the autophagy and mTORC1 pathways specifically in TNBCs, while the link between *GPT2* and mTORC1 seems to be relevant even across all subtypes of breast cancer. Taken together our results demonstrate that there is a robust network connecting mTORC1, autophagy and glutaminolytic pathways with *GPT2* alanine aminotransferase activity that likely helps to maintain amino acid levels in TNBC cancer and thereby promotes proliferation as well as sustains cell growth.

In conclusion, our findings show that *GPT2* has a prominent function particularly in TNBC, the most aggressive subtype lacking any targeted therapy. While its role in aiding glutamine-dependent anaplerosis has been mostly established, our study demonstrates that perturbing this pathway leads to the rewiring of glucose utilization within tumor cells that involves the activation of an alternative anaplerotic pathway catalyzed by pyruvate carboxylase. Combinatorial targeting of PC with glutamine metabolism inhibitors might thus be an interesting strategy for the treatment of breast cancer similar to glioblastoma cells where pyruvate carboxylase has been shown as an alternative route for carbon delivery to the TCA cycle under conditions of glutamine starvation and has been discussed as a route for resistance to inhibition of glutaminolysis.<sup>40</sup> Our study shows for the first time that *GPT2* modulates the counterbalancing forces of autophagy and mTORC1 activity not only in vitro, but also in vivo and in patients. Higher *GPT2* levels in patients correlate with markers of inhibited autophagy and poorer outcome and it is plausible to hypothesize that new treatments for TNBC patients with elevated *GPT2* might include modulators of the *GPT2*-mTORC1-autophagy pathway.

## ACKNOWLEDGMENTS

We thank Prof. Noboru Mizushima for kindly providing GFP-LC3 plasmids. We thank the Microarray Unit of the DKFZ Genomics and Proteomics Core Facility for performing excellent services. This work was supported by the German Federal Ministry of Education and Research (e:Med-FKZ: 031A429; e:Bio-FKZ: 0316168), the European Union's Horizon 2020 research and innovation program under the Marie Skłodowska-Curie grant agreement (EpiPredict-642 691) and the NCT-DTK School of Oncology Fellowship. The authors acknowledge financial support by the Helmholtz European Partnering Program for

the cooperation between DKFZ and NHRF to build the Athens Comprehensive Cancer Center (ACCC). All these study sponsors have no roles in the study design, the collection, analysis and interpretation of data. Open Access funding enabled and organized by ProjektDEAL.

### CONFLICT OF INTEREST

Aristotelis Chatziioannou is the Chief Executive Officer of e-NIOS Application PC.

### DATA AVAILABILITY STATEMENT

All microarray data generated and analyzed in the course of this study have been uploaded to the ArrayExpress (<https://www.ebi.ac.uk/arrayexpress/>) and are available via the accession number E-MTAB-7680 and E-MTAB-7541. The authors declare that all data supporting the findings of this study are available within the article and its Supplementary Information file. All other data are available upon reasonable request by contacting the corresponding authors.

### ETHICS STATEMENT

Human primary breast cancer samples were collected at the Martin-Luther University, Halle-Wittenberg between 2009 and 2011 as part of the multicenter prospective PiA cohort (NCT 01592825). The study was approved by the ethics committee of the Martin-Luther University Halle-Wittenberg and informed consent was obtained from each patient. Our study is in accordance with the Declaration of Helsinki. The animal experiments were performed according to the national guidelines and were approved first by an institutional animal welfare officer of the German Cancer Research Center Heidelberg, Germany. All experiments were in addition approved by the responsible national authority, the local Governmental Committee for Animal Experimentation (Regierungspräsidium Karlsruhe, Germany) under the license G288-14.

### ORCID

Silvia Vega-Rubin-de-Celis  <https://orcid.org/0000-0002-4196-8996>

Stefan Wiemann  <https://orcid.org/0000-0003-4683-3174>

### REFERENCES

- Dai X, Li T, Bai Z, et al. Breast cancer intrinsic subtype classification, clinical use and future trends. *Am J Cancer Res*. 2015;5:2929-2943.
- DeBerardinis RJ, Chandel NS. Fundamentals of cancer metabolism. *Sci Adv*. 2016;2:e1600200.
- Ward PS, Thompson CB. Metabolic reprogramming: a cancer hallmark even Warburg did not anticipate. *Cancer Cell*. 2012;21:297-308.
- Warburg O, Wind F, Negelein E. The metabolism of tumors in the body. *J Gen Physiol*. 1927;8:519-530.
- DeBerardinis RJ, Cheng T. Q's next: the diverse functions of glutamine in metabolism, cell biology and cancer. *Oncogene*. 2010;29:313-324.
- Smith B, Schafer XL, Ambeskovic A, Spencer CM, Land H, Munger J. Addiction to coupling of the Warburg effect with glutamine catabolism in Cancer cells. *Cell Rep*. 2016;17:821-836.
- Hao Y, Samuels Y, Li Q, et al. Oncogenic PIK3CA mutations reprogram glutamine metabolism in colorectal cancer. *Nat Commun*. 2016;7:11971.
- Tan HWS, Sim AYL, Long YC. Glutamine metabolism regulates autophagy-dependent mTORC1 reactivation during amino acid starvation. *Nat Commun*. 2017;8:338.
- Nicklin P, Bergman P, Zhang B, et al. Bidirectional transport of amino acids regulates mTOR and autophagy. *Cell*. 2009;136:521-534.
- Lampa M, Arlt H, He T, et al. Glutaminase is essential for the growth of triple-negative breast cancer cells with a deregulated glutamine metabolism pathway and its suppression synergizes with mTOR inhibition. *PLoS One*. 2017;12:e0185092.
- Zhu Y, Lin G, Dai Z, et al. L-glutamine deprivation induces autophagy and alters the mTOR and MAPK signaling pathways in porcine intestinal epithelial cells. *Amino Acids*. 2015;47:2185-2197.
- Galluzzi L, Pietrocola F, Levine B, Kroemer G. Metabolic control of autophagy. *Cell*. 2014;159:1263-1276.
- Russell RC, Yuan HX, Guan KL. Autophagy regulation by nutrient signaling. *Cell Res*. 2014;24:42-57.
- Bernhardt S, Bayerlova M, Vetter M, et al. Proteomic profiling of breast cancer metabolism identifies SHMT2 and ASCT2 as prognostic factors. *Breast Cancer Res*. 2017;19:112.
- von Minckwitz G, Untch M, Blohmer JU, et al. Definition and impact of pathologic complete response on prognosis after neoadjuvant chemotherapy in various intrinsic breast cancer subtypes. *J Clin Oncol*. 2012;30:1796-1804.
- Goldhirsch A, Winer EP, Coates AS, et al. Personalizing the treatment of women with early breast cancer: highlights of the St Gallen international expert consensus on the primary therapy of early breast Cancer 2013. *Ann Oncol*. 2013;24:2206-2223.
- Yuan JS, Reed A, Chen F, Stewart CN Jr. Statistical analysis of real-time PCR data. *BMC Bioinformatics*. 2006;7:85.
- Shi W, Oshlack A, Smyth GK. Optimizing the noise versus bias trade-off for Illumina whole genome expression BeadChips. *Nucleic Acids Res*. 2010;38:e204.
- Du P, Kibbe WA, Lin SM. lumi: a pipeline for processing Illumina microarray. *Bioinformatics*. 2008;24:1547-1548.
- Ritchie ME, Phipson B, Wu D, et al. Limma powers differential expression analyses for RNA-sequencing and microarray studies. *Nucleic Acids Res*. 2015;43:e47.
- Koutsandreas T, Binenbaum I, Pilalis E, Valavanis I, Papadodima O, Chatziioannou A. Analyzing and visualizing genomic complexity for the derivation of the emergent molecular networks. *Int J Monit Surv Technol Res*. 2016;4:30-49.
- Subramanian A, Tamayo P, Mootha VK, et al. Gene set enrichment analysis: a knowledge-based approach for interpreting genome-wide expression profiles. *Proc Natl Acad Sci USA*. 2005;102:15545-15550.
- Reich M, Liefeld T, Gould J, Lerner J, Tamayo P, Mesirov JP. GenePattern 2.0. *Nat Genet*. 2006;38:500-501.
- Loebke C, Suelmann H, Schmidt C, et al. Infrared-based protein detection arrays for quantitative proteomics. *Proteomics*. 2007;7:558-564.
- Mannspenger HA, Gade S, Henjes F, Beissbarth T, Korf U. RPPanalyzer: analysis of reverse-phase protein array data. *Bioinformatics*. 2010;26:2202-2203.
- Pietzke M, Kempa S. Pulsed stable isotope-resolved metabolomic studies of cancer cells. *Methods Enzymol*. 2014;543:179-198.
- Kuich PH, Hoffmann N, Kempa S. Maui-VIA: a user-friendly software for visual identification, alignment, correction, and quantification of gas chromatography-mass spectrometry data. *Front Bioeng Biotechnol*. 2014;2:84.
- Mizushima N, Yamamoto A, Matsui M, Yoshimori T, Ohsumi Y. In vivo analysis of autophagy in response to nutrient starvation using transgenic mice expressing a fluorescent autophagosome marker. *Mol Biol Cell*. 2004;15:1101-1111.
- Gross MI, Demo SD, Dennison JB, et al. Antitumor activity of the glutaminase inhibitor CB-839 in triple-negative breast cancer. *Mol Cancer Ther*. 2014;13:890-901.



30. Korangath P, Teo WW, Sadik H, et al. Targeting glutamine metabolism in breast cancer with aminooxyacetate. *Clin Cancer Res.* 2015;21:3263-3273.
31. Curtis C, Shah SP, Chin SF, et al. The genomic and transcriptomic architecture of 2,000 breast tumours reveals novel subgroups. *Nature.* 2012;486:346-352.
32. Cancer Genome Atlas Network. Comprehensive molecular portraits of human breast tumours. *Nature.* 2012;490:61-70.
33. Riaz M, van Jaarsveld MT, Hollestelle A, et al. miRNA expression profiling of 51 human breast cancer cell lines reveals subtype and driver mutation-specific miRNAs. *Breast Cancer Res.* 2013;15:R33.
34. Thuwajit C, Ferraresi A, Titone R, Thuwajit P, Isidoro C. The metabolic cross-talk between epithelial cancer cells and stromal fibroblasts in ovarian cancer progression: autophagy plays a role. *Med Res Rev.* 2018;38:1235-1254.
35. Vega-Rubín-de-Celis S, Wiemann S. Autophagy LC3 HiBiT reporter assay system demonstrates mTORC1 regulation of autophagic flux. *Promega Corporation.* 2018;tpub\_204.
36. Pavlova NN, Thompson CB. The emerging hallmarks of Cancer metabolism. *Cell Metab.* 2016;23:27-47.
37. van Geldermalsen M, Wang Q, Nagarajah R, et al. ASCT2/SLC1A5 controls glutamine uptake and tumour growth in triple-negative basal-like breast cancer. *Oncogene.* 2016;35:3201-3208.
38. Coloff JL, Murphy JP, Braun CR, et al. Differential glutamate metabolism in proliferating and quiescent mammary epithelial cells. *Cell Metab.* 2016;23:867-880.
39. Whalen WA, Wang MD, Berg CM. Beta-Chloro-L-alanine inhibition of the *Escherichia coli* alanine-valine transaminase. *J Bacteriol.* 1985;164:1350-1352.
40. Cheng T, Sudderth J, Yang C, et al. Pyruvate carboxylase is required for glutamine-independent growth of tumor cells. *Proc Natl Acad Sci USA.* 2011;108:8674-8679.
41. Christen S, Lorendeau D, Schmieder R, et al. Breast cancer-derived lung metastases show increased pyruvate carboxylase-dependent anaplerosis. *Cell Rep.* 2016;17:837-848.
42. Levine B, Klionsky DJ. Development by self-digestion: molecular mechanisms and biological functions of autophagy. *Dev Cell.* 2004;6:463-477.
43. Klionsky DJ, Emr SD. Autophagy as a regulated pathway of cellular degradation. *Science.* 2000;290:1717-1721.
44. Mamane Y, Petroulakis E, LeBacquer O, Sonenberg N. mTOR, translation initiation and cancer. *Oncogene.* 2006;25:6416-6422.
45. Magnuson B, Ekim B, Fingar DC. Regulation and function of ribosomal protein S6 kinase (S6K) within mTOR signalling networks. *Biochem J.* 2012;441:1-21.
46. Cluntun AA, Lukey MJ, Cerione RA, Locasale JW. Glutamine metabolism in cancer: understanding the heterogeneity. *Trends Cancer.* 2017;3:169-180.

### SUPPORTING INFORMATION

Additional supporting information may be found online in the Supporting Information section at the end of this article.

**How to cite this article:** Mitra D, Vega-Rubin-de-Celis S, Royle N, et al. Abrogating GPT2 in triple-negative breast cancer inhibits tumor growth and promotes autophagy. *Int. J. Cancer.* 2021;148:1993-2009. <https://doi.org/10.1002/ijc.33456>